Published in final edited form as:

Nat Immunol. 2018 February ; 19(2): 173–182. doi:10.1038/s41590-017-0029-3.

Intravital mucosal imaging of CD8+ resident memory T cells shows tissue-autonomous recall responses that amplify secondary memory

Lalit K. Beura[1,2], **Jason S. Mitchell**[2,3], **Emily A. Thompson**[1,2], **Jason M. Schenkel**[1,2], **Javed Mohammed**[4], **Sathi Wijeyesinghe**[1,2], **Raissa Fonseca**[1,2], **Brandon J. Burbach**[2,3], **Heather D. Hickman**[5], **Vaiva Vezys**[1,2], **Brian T. Fife**[2,6], and **David Masopust**[1,2,*]

[1]Department of Microbiology and Immunology, University of Minnesota, Minneapolis, MN, USA

[2]Center for Immunology, University of Minnesota, Minneapolis, MN, USA

[3]Department of Laboratory Medicine and Pathology, University of Minnesota, Minneapolis, MN, USA

[4]Department of Dermatology, University of Minnesota, Minneapolis, MN, USA

[5]Viral Immunity and Pathogenesis Unit, Laboratory of Clinical Immunology and Microbiology, National Institute of Allergy and Infectious Diseases, US National Institutes of Health, Bethesda, MD, USA

[6]Department of Medicine, University of Minnesota, Minneapolis, MN, USA

Abstract

CD8$^+$ T cell immunosurveillance dynamics influence the outcome of intracellular infections and cancer. Here we used two-photon intravital microscopy to visualize the responses of CD8$^+$ resident memory T cells (T_{RM} cells) within the reproductive tracts of live female mice. We found that mucosal T_{RM} cells were highly motile, but paused and underwent in situ division after local antigen challenge. T_{RM} cell reactivation triggered the recruitment of recirculating memory T cells that underwent antigen-independent T_{RM} cell differentiation in situ. However, the proliferation of pre-existing T_{RM} cells dominated the local mucosal recall response and contributed most substantially to the boosted secondary T_{RM} cell population. We observed similar results in skin. Thus, T_{RM} cells can autonomously regulate the expansion of local immunosurveillance independently of central memory or proliferation in lymphoid tissue.

* masopust@umn.edu.

Author contributions

L.K.B., J.S.M., E.A.T., J.M.S., J.M., S.W, R.F. and B.J.B. performed the experiments; H.D.H., V.V. and B.T.F. contributed critical reagents and experimental help; L.K.B., J.S.M. and E.A.T. analyzed intravital microscopy data; L.K.B. and D.M. wrote the manuscript; and D.M. was responsible for research supervision, coordination and strategy.

Competing interests

The authors declare no competing financial interests.

Supplementary information is available for this paper at https://doi.org/10.1038/s41590-017-0029-3.

Naive T cells limit immunosurveillance to secondary lymphoid organs (SLOs) such as lymph nodes (LNs) through a restricted pattern of recirculation via blood and lymph vessels. Upon antigen encounter in LNs, naive T cells undergo rapid proliferation, giving rise to differentiated effector T cells and long-lived memory T cells that are distributed more broadly throughout the body. Memory T cells are grouped into subsets on the basis of the anatomic locations they patrol and their perceived functional role in the event of reinfection[1,2]. Central memory T cells (T_{CM} cells), similarly to naive T cells, patrol LNs and seem to be specialized to proliferate in the event of reinfection, in this case when pathogen-derived antigens reach SLOs. T_{CM} cells produce abundant secondary effector T cells that migrate to nonlymphoid sites of infection and also give rise to expanded populations of long-lived memory T cells[2,3]. Effector memory T cells (T_{EM} cells) generally patrol regions outside of LNs and are typically thought of as terminally differentiated peripheral surveyors poised for rapid expression of effector functions, but not secondary expansion[4–6]. Both T_{CM} cells and T_{EM} cells recirculate, meaning they can be found in blood. T_{RM} cells[7], a third major population of memory T cells, are parked in tissues, where they accelerate clearance of local reinfections, and thus are absent from blood[7,8].

Because T_{RM} cells share properties with effector T cells and T_{EM} cells, potentially including the expression of CD69 and granzyme B and the absence of LN homing receptors such as CD62L, the prevailing view is that T_{RM} cells are also terminally differentiated, and thus are not responsible for expansion of their own population or boosting of local nonlymphoid tissue secondary memory T cell populations after reinfection. Rather, boosting of tissue memory is thought to require antigen trafficking to downstream lymphoid organs and proliferation and differentiation by the more ‘stem-cell-like’ T_{CM} cells. Indeed, when T_{RM} cells are restimulated outside of nonlymphoid tissues, expansion is poor compared with that of naive T cell or T_{CM} cell populations, which suggests that T cell intrinsic differences impair proliferation potential[9–11]. However, T_{RM} cells are difficult to study ex vivo because of their poor survival after being removed from tissues[12–14].

T_{RM} cells can trigger a tissue-wide state of pathogen resistance and immune stimulation, and precipitate the recruitment of recirculating lymphocytes to sites of T_{RM} cell reactivation[15,16]. However, the fate of recruited cells is unclear. Moreover, formal descriptions of the relationship between $CD8^+$ T cell magnitude, location and differentiation state and the efficiency of pathogen detection and clearance are in their infancy. Indeed, we lack in vivo data for mucosal T_{RM} cell motility, which is intrinsically related to the scanning rate of potential target cells. Intravascular T_{RM} cells that patrol liver sinusoids are motile, but it is unclear whether this is true of the numerous T_{RM} cells that survey connective tissues and parenchymal barriers[13]. Indeed, T_{RM} cell motility in skin epidermis is quite low (~2 μm min^{-1}), in contrast to that of T_{CM} cells surveilling LNs (~10 μm min^{-1})[15,17–19]. This suggests that resident populations of memory T cells not only do not migrate between tissues, but also may be relatively stationary within stromal or parenchymal tissues.

To address T_{RM} cell immunosurveillance in the mucosa, we developed an intravital two-photon microscopy model to image mouse uterus after acute lymphocytic choriomeningitis virus (LCMV) infection and combined it with depletion strategies, parabiosis and dual-challenge models to test the relative contributions of T_{RM} cells to secondary population

expansion after local anamnestic antigen exposure. We found that compared with circulating memory T cells, T_{RM} cells in both the female reproductive tract and the skin have the potential to dominate local recall responses and contribute most substantially to boosting of the secondary T_{RM} cell population. These data indicate that T_{RM} cells have the capacity to autonomously regulate the expansion of local immunosurveillance independently of T_{CM} cells or proliferation in lymphoid tissue.

Results

T cell motility accelerates after antigen clearance in the female reproductive tract

To establish a model for observing dynamic T cell behavior in the female reproductive tract (FRT) in living mice, we transferred GFP^+CD8^+ P14 T cell receptor-transgenic (P14) T cells, which are specific for the immunodominant gp33 epitope of LCMV, into naive C57BL/6 mice and then infected the recipients with 2×10^5 plaque-forming units of LCMV Armstrong intraperitoneally (i.p.). This resulted in LCMV infection of the FRT (Fig. 1a), as well as establishment of GFP^+ P14 T_{RM} cells in all three layers of the uterine horn[20–22] (Supplementary Fig. 1a,b) in the recipient mice (hereinafter referred to as GFP^+ P14 immune chimeras). Mice are multiparous and have relatively long uterine horns, which could be sufficiently exteriorized to be imaged under laser-scanning intravital two-photon microscopy (IV-2PM; Methods) while remaining intact within the mouse. Using this approach, we visualized the motility of LCMV-specific GFP^+ P14 T_{RM} cells within the uterine mucosa at different stages of LCMV infection. We focused all live imaging on the most superficial 200 μm, which was the optimal depth for use with the instrumentation and tissue properties in this experiment. Thus, our analyses were restricted to the perimetrium and myometrium, and did not include the endometrium or luminal epithelium.

At day 4.5 after LCMV infection, GFP^+ P14 T cell motility was approximately 6 μm min^{-1}, with some GFP^+ P14 T cells arrested (Fig. 1b–d and Supplementary Video 1). Motility increased to ~10 μm min^{-1} by day 8 after infection, which coincided with the time of observable antigen clearance after LCMV Armstrong infection in mice (Fig. 1a and Supplementary Video 2). At day 30 after LCMV infection, at which time T cells in the FRT are almost exclusively T_{RM} cells[12,21], GFP^+ P14 T cell motility remained high at ~10 μm min^{-1} (Supplementary Video 3). Antigen clearance was also accompanied by an increase in the motility coefficient, expressed as the rate of GFP^+ P14 T cell displacement from the starting position (Fig. 1c). These data suggest that $CD8^+$ T_{RM} cell motility in the stroma of the FRT is much faster than that reported in skin epidermis (2 μm min^{-1})[17]. The motility of GFP^+ OT-I memory T cells, which recognize the ovalbumin (OVA)-derived peptide SIINFEKL, established in the FRT 60 d after infection with either vesicular stomatitis virus (VSV) or vaccinia virus (VV) expressing OVA (VSV-OVA or VV-OVA, respectively) was also ~10 μm min^{-1} (Fig. 1e).

The discrepancy in motility that we observed between the FRT and what has been reported for skin epidermis, which comprises compacted layers of flattened cells, could be due to the difference in tissue architecture. We found that the motility of GFP^+ P14 T cells was lower (~6 μm min^{-1}) in the perimetrium (the outer serosal lining of the uterus) and the subjacent thin layer of dense connective tissue than in the myometrium (the muscular layer of the

uterus; ~10 μm min^{-1}) (Supplementary Fig. 2). In fact, the average speed of GFP^+ P14 T cells migrating in less collagen-rich areas (tracks > 2 μm away from second harmonic generation (SHG) signals) was significantly faster than that of cells close to collagen-dense regions (< 2 μm from SHG signals; Fig. 1f,g). In summary, both antigen and location have a role in $CD8^+$ T cell migration within the uterine stroma.

Local reactivation results in motility arrest of T_{RM} cells

Previous studies indicated that > 99% of LCMV-Armstrong-specific P14 $CD8^+$ T cells within the FRT are resident at any time point 1–8 months after LCMV infection, 60–75% of T_{RM} cells in the FRT express CD69, and only a minority express CD103[12]. To test whether T_{RM} cell motility is affected by local antigen detection, which could influence subsequent immunosurveillance rates, we used mice that had received adoptively transferred GFP^+ P14 T cells and been infected with LCMV Armstrong as described above, and we deposited LCMV-gp33 peptide into the lumen of the cervix (trans-cervical delivery) in these mice 60 d after primary LCMV infection. Corresponding with T_{RM} cell reactivation[16,21], we observed changes in dendritic cell morphology and a reduction in the average motility of GFP^+CD8^+ P14 T cells from 10.1 μm min^{-1} at steady state to 5.3 μm min^{-1} within 12 h (Fig. 2a,b and Supplementary Videos 4 and 5). These motility changes were transient, as GFP^+CD8^+ P14 T cells resumed their previous migration behavior with respect to both mean track speed and motility coefficient within 48 h after gp33 exposure (Fig. 2b).

We next tested whether T_{RM} cell motility arrest is dependent on stimulation by cognate antigen or is a result of bystander effects of local peptide exposure and/or neighboring T_{RM} cell activation. To generate mice with traceable T_{RM} cells with discrete antigenic specificities, we adoptively transferred GFP^+ OT-I T cells into cyan fluorescent protein (CFP)-expressing P14 immune chimeras 30 d after LCMV infection, and then infected the chimeras with VSV-OVA. Thirty days after VSV-OVA infection, we exposed the CFP^+ $P14{-}GFP^+$ OT-I immune chimeric mice to gp33 peptide locally through trans-cervical rechallenge, and monitored the mean track speeds of CFP^+ P14 T cells and GFP^+CD8^+ OT-I T cells simultaneously (Supplementary Video 6). Only the migration of CFP^+ P14 T cells was reduced at 12 h compared with that of resting OT-I $CD8^+$ memory T cells that did not recognize recall antigen (Fig. 2c,d), which indicated that T_{RM} cell motility arrest depends on cognate-antigen-specific T-cell-receptor-mediated signals, rather than bystander effects.

In situ division in the female reproductive tract

Next, we assessed the dynamics of the response in the FRT after local antigen rechallenge by infecting mice carrying adoptively transferred P14 $CD8^+$ T cells with LCMV Armstrong and then subjecting them to transcervical rechallenge with gp33 60 d after LCMV infection. IV-2PM monitoring of the recall response indicated the accumulation of GFP^+ P14 T cells in the uterine mucosa 36 and 48 h after gp33 peptide inoculation (Fig. 3a,b). We observed hundreds of GFP^+ P14 T cells undergoing in situ division at 36 h after gp33 peptide inoculation, with rare examples as early as 32 h (Fig. 3c and Supplementary Video 7). Consistent with this observation, P14 $CD8^+$ T cells in the FRT were $Ki67^+$ 48 h after local rechallenge, which indicates that they were undergoing proliferation (Fig. 3d,f and Supplementary Fig. 1c,d). The mice were also i.p. pulsed with 5-bromo-2′-deoxy-uridine

(BrdU) 2 h before they were killed. By 2 h after BrdU treatment, ~25% of P14 $CD8^+$ T cells had incorporated BrdU (Fig. 3d), which indicated that they were undergoing active DNA synthesis and thus confirmed that they were proliferating.

Transgenic fluorophore-expressing $CD8^+$ T cells are necessary for IV-2PM visualization of antigen-specific responses. To determine whether the division of GFP^+ P14 T cells was an artifact of adoptive transfer, we immunized C57BL/6 J (B6; 'wild-type') mice with LCMV, rechallenged the mice with gp33 peptide trans-cervically 90 d after infection, and measured Ki67 expression and BrdU incorporation in endogenous LCMV-specific $CD8^+$ T cells detected with H-$2D^b$/gp33 MHC I tetramers (Supplementary Fig. 3). Tetramer-positive cells became $Ki67^+$ and $BrdU^+$, which indicates that antigen-specific T_{RM} cells divide in the FRT after local rechallenge. To test whether in situ division of T_{RM} cells occurs in response to live replicating virus, we transferred naive $CD45.1^+CD8^+$ OT-I T cells into naive B6 recipients and then immunized them with VSV-OVA. Ninety days later, we challenged the mice trans-cervically with VV-OVA or VV expressing gp33 epitope (VV-gp33). $CD45.1^+CD8^+$ OT-I T cells became $Ki67^+$ and/or $BrdU^+$ in response to cognate-antigenbearing viral rechallenge, which indicates that live replicating virus induced division by antigen-specific $CD8^+$ T cells within the FRT (Fig. 3e,g). Lastly, we assessed the relationship between motility and division. Two months after primary LCMV infection, we challenged GFP^+ P14 immune chimeras with LCMV-gp33 peptide trans-cervically, and 36 h after gp33 recall we used intravital microscopy to monitor the motility of GFP^+ P14 T cells undergoing active division compared with that of GFP^+ P14 T cells that were not dividing in a 15-min period. Dividing GFP^+ P14 T cells underwent a transient reduction in motility, then regained rapid motility after cytokinesis was completed (Fig. 3h,i and Supplementary Video 7). In summary, these data indicate that antigen-specific memory T cells in the FRT undergo pausing and cytokinesis after local antigen rechallenge.

T_{RM} cells divide in the female reproductive tract after reactivation

We next investigated whether T_{RM} cells in the FRT undergo division in situ, or whether antigen rechallenge induces the division of only antigen-specific T cells newly recruited from the blood, such as T_{CM} cells. Using mice that had previously received adoptively transferred GFP^+ P14 T cells and been infected with LCMV Armstrong as described above, we administered anti-CD90.1 titrated to induce depletion of blood P14 $CD8^+$ T cells, but insufficient to deplete P14 $CD8^+$ T cells confined within the FRT. A single dose of anti-CD90.1 caused P14 $CD8^+$ T cells to be almost completely eliminated from blood, LNs and spleen while remaining abundant in the FRT (Fig. 4a). We additionally blocked the migration of circulating P14 $CD8^+$ T cells into the FRT by injecting anti-VCAM-1 and anti-CD49d 24 h before and 24 h after trans-cervical challenge with $gp33^{16}$. For proliferation monitoring, we administered BrdU i.p. 2 h before we collected P14 $CD8^+$ T cells from the FRT. We observed that 24 and 36 h after gp33 challenge, P14 $CD8^+$ T cells in the FRT of mice treated with anti-CD90.1, anti-VCAM-1 and anti-CD49d showed equivalent BrdU incorporation and Ki67 upregulation compared with T cells in challenged mice that did not receive antibodies (Fig. 4b,c). In addition, intravital microscopy showed GFP^+ P14 T cell proliferation in situ in GFP^+ P14 immune chimeras treated with these antibodies

(Supplementary Video 8). These results indicate that P14 CD8$^+$ T_{RM} cells rapidly initiate in situ proliferation in the FRT mucosa after anamnestic challenge.

It was previously shown that help from CD4$^+$ T cells is required to promote CD8$^+$ T cell migration to the mouse FRT and to establish local CD8$^+$ T cell memory after infection with a thymidine-kinase-deficient strain of herpes simplex virus (HSV) type 2[23]. However, CD4$^+$ T cell help is dispensable for the establishment of skin CD8$^+$ T_{RM} cells after exposure to VV[24]. Moreover, CD4$^+$ T cell help has been reported to be important for priming memory CD8$^+$ T cells that retain proliferative potential, although this has not been addressed for T_{RM} cells[25,26]. Thus we addressed whether the establishment of T_{RM} cells in the FRT requires help from CD4$^+$ T cells after infection with LCMV, by transferring naive P14 CD8$^+$ T cells into MHC-II-deficient recipients and then infecting them with LCMV Armstrong 1 d after cell transfer. We collected P14 CD8$^+$ T cells from the FRT of MHC-II-deficient mice and from wild-type B6 mice 40 d after infection, and found that the cell numbers were similar in both groups of mice (Supplementary Fig. 4). We observed similar results at 7 d after LCMV infection and in *Cd4*$^{-/-}$ mice (data not shown and Supplementary Fig. 4). Next, we depleted the circulating P14 CD8$^+$ T cells with anti-CD90.1 (administered i.p. 96 h before rechallenge) and blocked de novo migration into the FRT with anti-VCAM-1 and anti-CD49d (administered i.p. 1 d before the rechallenge) in wild-type and MHC-II-deficient P14 immune chimeras, and then rechallenged the mice with gp33 trans-cervically. Upregulation of Ki67 by CD90.1$^+$CD8$^+$ P14 T cells was equivalent (~40%) in wild-type and MHC-II-deficient mice (Fig. 4d), which suggests that CD90.1$^+$CD8$^+$ P14 T cells did not require CD4$^+$ T cell help during either priming or reactivation to initiate entry into the cell cycle. We also tested the requirement for CD11c$^+$ cells, which include dendritic cells, for T_{RM} cell reactivaion. We irradiated B6 mice and then transplanted bone marrow from CD11c-DTR mice, in which CD11c$^+$ cells express the diphtheria toxin (DT) receptor. Two months later, we delivered adoptively transferred CD90.1$^+$CD8$^+$ P14 T cells into the CD11c-DTR chimeric mice and infected them with LCMV Armstrong. Sixty days after LCMV infection, we began treating the mice with DT, with administration every 2 d starting at 48 h before trans-cervical rechallenge with gp33, which resulted in depletion of ~90% of CD11c$^+$ cells in the FRT (Supplementary Fig. 4d). Twenty-four hours after gp33 challenge, ~35% of P14 CD8$^+$ T cells upregulated Ki67 at similar levels in DT-treated and untreated control mice (Fig. 4e). These results indicate that bona fide T_{RM} cells were triggered to undergo proliferation in situ after mucosal tissue rechallenge, and that this process did not depend on CD4$^+$ T cell help and was probably independent of CD11c$^+$ host cells.

Recruited circulating bystanders convert to T_{RM} cells

T_{RM} cell reactivation in the mucosa induces rapid upregulation of inflammatory homing molecules, which results in local recruitment of circulating memory T cells in a chemokine- and integrin-dependent process[21]. However, the long-term fate of these newly recruited bystander CD8$^+$ T cells is unknown. To address this issue, we isolated memory OT-I CD8$^+$ T cells from the spleen and LNs of mice that had been infected with VSV-OVA at least 60 d prior and transferred them i.v. into mice that had received adoptively transferred P14 CD8$^+$ T cells and been infected with LCMV Armstrong at least 60 d prior. We then subjected these mice to trans-cervical rechallenge with gp33 1 d after memory OT-I CD8$^+$ T cell transfer. At

45 and 75 d after gp33 rechallenge, we detected the accumulation of CD45.1$^+$CD8$^+$ OT-I T cells in the FRT of recipient CD90.1$^+$ P14 immune chimeric mice that were challenged with LCMV-gp33 trans-cervically, compared with cell numbers in PBS-challenged mice (Fig. 5a). A substantive fraction of the CD45.1$^+$CD8$^+$ OT-I T cells were CD69$^+$, although 60% were CD69$^-$, and very few expressed CD103 (Fig. 5b,c). Despite this phenotypic heterogeneity, we assessed whether the recruited OT-I CD8$^+$ T cells were resident by transferring circulating memory CD45.1$^+$CD8$^+$ OT-I T cells into CD90.1$^+$ P14 immune chimeric mice and then challenging the mice with gp33 peptide trans-cervically to recruit the OT-I CD8$^+$ T cells to the FRT. Forty days after gp33 challenge, we surgically joined these mice with naive B6 mice (Fig. 5d). At 35 d after parabiosis, we could not detect any CD45.1$^+$CD8$^+$ OT-I T cells in the FRTs of the naive parabiotic partners (Fig. 5e), which indicated that almost all bystander memory OT-I T cells retained were resident. These data suggest that induction of the T_{RM} cell program within the FRT does not absolutely require local cognate antigen recognition, that recirculating memory T cells retain the developmental potential to differentiate into T_{RM} cells, and that periodic reinfection events may induce bystander memory T cell redistribution out of circulation and into mucosal tissues.

T_{RM} cell proliferation dominates expansion of local secondary memory

Local exposure to anamnestic antigen resulted in rapid and profound population expansion of mucosal antigen-specific T cells (Fig. 3). This recall response could have been dominated by non-T_{RM} cells (for example, T_{CM} cells that were reactivated in the draining LN or were newly recruited to the FRT) or in situ expansion of preformed T_{RM} cells. To distinguish among these possibilities, we adoptively transferred naive CD8$^+$ T cells from CD45.1$^+$ P14 mice or CD90.1$^+$ P14 mice into CD45.2$^+$CD90.2$^+$ C57BL/6 recipient mice and infected those recipients with LCMV the following day. Sixty days after LCMV infection, we carried out parabiotic surgery to join CD45.1$^+$ P14 mice and CD90.1$^+$ P14 immune chimeric mice, and we allowed 14–30 d after surgery to induce equilibration of circulating P14 CD8$^+$ T cells before proceeding to trans-cervical challenge with gp33 in both mice of the parabiotic pair (Supplementary Fig. 5). As shown by both flow cytometry and quantitative immunofluorescence microscopy (QIM), the ratios of CD45.1$^+$CD8$^+$ P14 T cells to CD90.1$^+$CD8$^+$ P14 T cells were similar in the spleens of both mice in the parabiotic pair 2 d after gp33 challenge (Fig. 6a,b). In contrast, in the FRT compartment, host P14 CD8$^+$ T cells dominated over parabiotic-partner-derived P14 CD8$^+$ T cells (Fig. 6b,c), even though the total number of P14 CD8$^+$ T cells in the FRT had increased tenfold (Fig. 6d), which indicated that 2 d after local rechallenge most of the accumulating antigen-specific T cells were derived from T_{RM} cells. Consistent with this interpretation, at this early time point, most host-derived P14 CD8$^+$ T cells in the FRT expressed markers of T_{RM} cells (particularly CD69), in contrast to parabiont-partner-derived P14 CD8$^+$ T cells (Fig. 6a). The disequilibrium between host and donor-derived P14 CD8$^+$ T cells in the FRT was more pronounced 30 d after local challenge (the host/parabiont-partner-derived P14 CD8$^+$ T cell ratio was ~10:1 at day 2, compared with ~24:1 at day 30) (Fig. 6c,e–g), which suggests that T_{RM} cells locally expanding during the effector phase of the response had a greater propensity to differentiate into secondary memory T_{RM} cells compared with recirculating memory T cells. We observed an approximately threefold increase in the number of total

memory T cells (combined host and parabiont-partner-derived P14 $CD8^+$ T cells) in the FRT 30 d after rechallenge (Fig. 6d), with the host/parabiont-partner P14 $CD8^+$ T cell ratio highly biased in favor of the host cells (Fig. 6g). These data demonstrate that at least in this reductionist setting, T_{RM} cells can contribute substantively to secondary effector accumulation and local anamnestic memory.

To extend our analysis to a different rechallenge model and a different anatomic site, we adoptively transferred either $CD45.1^+CD8^+$ OT-I T cells or $CD90.1^+CD8^+$ OT-I T cells into C57BL/6 mice and then infected the mice i.v. with VSV-OVA, which induced the generation of OT-I memory $CD8^+$ T cells in both the FRT and the skin (Supplementary Fig. 6). Thirty days after VSV-OVA infection, we established parabiotic pairs, each consisting of one mouse that had received transferred $CD45.1^+$ OT-I T cells and one that had received $CD90.1^+$ OT-I T cells, and allowed equilibration of circulating OT-I $CD8^+$ T cells for 14–30 d. We then rechallenged each conjoined parabiont locally with modified VV Ankara expressing the immunodominant SIINFEKL epitope derived from OVA (MVA-OVA) via either the trans-cervical (Fig. 7a–c) or the epicutaneous route[27] (Fig. 7d–f). One month later, we used QIM to examine the expansion and origin of OT-I $CD8^+$ T cell populations in each mouse's FRT or skin. There were approximately ninefold more host-derived OT-I $CD8^+$ T cells than parabiotic-partner-derived OT-I $CD8^+$ T cells in both FRT (Fig. 7b) and skin (Fig. 7e), which indicated that local FRT or skin challenge with MVA-OVA resulted in local amplification of host-derived T_{RM} cell populations. These data suggest that T_{RM} cells may autonomously amplify local immune surveillance and memory in various barrier sites in response to a range of stimuli.

Discussion

This study demonstrates that $CD8^+$ T_{RM} cells within the stroma of the FRT exhibit motility rates that are similar to those of circulating lymphocytes in LNs. In response to local re-encounter with cognate antigen, T_{RM} cells pause, then proliferate even in the absence of $CD4^+$ T cell help. In the contexts examined here, FRT and skin T_{RM} cells dominated the local recall response and made a greater contribution than did circulating memory T cell subsets, including T_{CM} cells, to the expansion of a long-lived anamnestic T_{RM} cell population. These data highlight nonlymphoid-tissue-autonomous amplification of adaptive immune responses.

We observed that T_{RM} cells patrolled with a speed of 10 μm min^{-1} within the FRT myometrium, similar to the motility rate observed in SLOs. Unlike uterine myometrium and SLOs, the epidermis is densely populated with stationary keratinocytes, which suggests that motility may be partly regulated by tissue architecture[28,29]. Indeed, we found that motility was substantially reduced (~6 μm min^{-1}) in the matrix-dense region of the uterine perimetrium. These observations argue against the concept that T_{RM} cells are necessarily stationary within tissues and reveal the marked heterogeneity of T_{RM} cell immunosurveillance patterns, which has important implications for modeling the requirements for immunity at frontline tissues.

It has been reported that after HSV infection in mice, effector $CD4^+$ T cells are required to migrate to the FRT before $CD8^+$ T cells can enter[23]. This important observation, if generalized, suggests that cytotoxic T lymphocyte responses to nonlymphoid tissues are intrinsically delayed, and thus are likely to impede the rapidity of viral control. It is therefore important to note that we observed no impairment in the migration of $CD8^+$ effector T cells (or the establishment of $CD8^+$ T_{RM} cells) to the FRT after LCMV infection in mice that lacked $CD4^+$ T cells, similar to what has been shown recently in an intracerebral LCMV infection model[30].

Our observations confirmed previous reports that T_{RM} cell reactivation induces the recruitment of bystander (non-antigen-specific) memory T cells to sites of ongoing infection[21,31,32]. In the current study, we found that some recruited bystander $CD8^+$ T cells persisted for more than 75 d in the nonlymphoid site of recruitment. This suggests that T cell migration from recirculating to resident compartments could be more dynamic in organisms that experience frequent recall infections (unlike laboratory mice that live in specific-pathogen-free facilities). Antigen encounter in non-lymphoid tissues has a role in shaping T_{RM} cell development, but the rules are unclear and seem to be tissue specific[20,33–35], although this issue has not been well addressed in the FRT. We found that a fraction of recruited bystander memory $CD8^+$ T cells upregulated CD69, but not CD103. Thus, cognate antigen recognition in tissue was clearly not required for CD69 induction. It remains unclear whether bystander recruited T cells, which include T_{CM} cells and T_{EM} cells, had lost the developmental capacity to fully acquire T_{RM} cell differentiation markers, or distribute differently, or whether local infection was required to enhance CD69 and CD103 induction signals[36]. The lineage relationship between T_{RM} cells and other memory T cell subsets is an area of active investigation.

The degree to which T_{RM} cells have the capacity for recall expansion in tissues also remains unclear[8]. Although some reports indicate that neither effector nor memory T cells divide within nonlymphoid tissues, an elegant study in the brain parenchyma challenged this view[37]. It showed that effector T cells could complete a division in situ, although those cells were pre-committed to divide (perhaps in the lymphoid tissue) prior to entry into the central nervous system[37]. Naive T cells can be primed in low-shear-flow vascular compartments, including the liver[38]. T cells can also be induced to divide within nonlymphoid tissue[39] by transplantation of the dorsal root ganglia of HSV-infected mice under the kidney capsule of naive mice, which induces viral reactivation. In this scenario, division depends on $CD4^+$ T cells and dendritic cells, which suggests that the rules for tissue division may be context dependent[39]. Here we found that T_{RM} cells in the FRT could be induced to undergo cell division in situ and complete antigen-induced cytokinesis within only 36 h of local stimulation. This was independent of $CD4^+$ T cell help, and was not impeded when 90% of $CDl1c^+$ cells were depleted. In addition, in situ T_{RM} cell proliferation dominated secondary expansion.

Residence provides a mechanism for regionalizing immunosurveillance by retaining cells in relevant locations, rather than relying on a tissue-restricted recirculation program. Our study extends this paradigm by revealing tissue-autonomous amplification of local memory, and suggests that iterative stimulation at a local site could enrich memory T cell

immunosurveillance at very specific sites. One important implication is that these recall responses would remain undetected if analysis were limited to blood. The clinical relevance of local self-amplifying T cell responses may extend beyond infectious disease[40,41], perhaps to include T-cell-driven autoimmune and allergic responses[7,42].

Methods

Methods, including statements of data availability and any associated accession codes and references, are available at https://doi.org/10.1038/s41590-017-0029-3.

Methods

Mice

C57BL/6 J (B6), C57BL/6-Tg(UBC-GFP)30Scha/J, B6.129(ICR)-Tg (CAG-ECFP)CK6Nagy/J, B6.129S2-*H2*$^{dlAb1\text{-}Ed}$/J (MHC II^{-}), B6.FVB-Tg(Itgax-DTR/EGFP)57Lan/J (CD11c-DTR), B6.Cg-Tg(Itgax-Venus)1Mnz/J (CD11c-YFP) and B6.SJL-Ptprc^{a}Pepc^{b}/BoyJ (CD45.1^{+}) female mice were from The Jackson Laboratory and were maintained in specific-pathogen-free conditions at the University of Minnesota. CD90.1^{+} P14, CD45.1^{+} P14 and CD45.1^{+} OT-I mice were fully backcrossed to C57BL/6 J mice and maintained in our animal colony. We generated P14 and OT-I reporter mice by crossing the mice with C57BL/6-Tg(UBC-GFP)30Scha/J or B6.129(ICR)-Tg(CAG-ECFP)CK6Nagy/J mice. Sample size was chosen on the basis of previous experience. No sample exclusion criteria were applied. No method of randomization was used during group allocation, and investigators were not blinded. All mice used in experiments were 6–14 weeks of age. All mice were used in accordance with the Institutional Animal Care and Use Committees guidelines at the University of Minnesota.

Adoptive transfers and infections

We generated P14 immune chimeras by transferring 5 × 10^{4} P14 CD8^{+} T cells into naive C57BL/6 J mice and then infecting those mice with 2 × 10^{5} plaque-forming units (PFU) of LCMV Armstrong i.p. 1 d later. For endogenous CD8^{+} T cell studies, we infected naive C57BL/6 J mice with 2 × 10^{5} PFU of LCMV Armstrong i.p., and we stained lymphocytes with H-2D^{b}/gp33 MHC I tetramers. We generated OT-I immune chimeras by transferring 5 × 10^{4} naive OT-I CD8^{+} T cells into C57BL/6 mice. We infected mice with 1 × 10^{6} PFU of vesicular stomatitis virus expressing chicken ovalbumin (VSV-OVA) i.v. We generated double-immune chimeras by seeding P14 immune chimeras with 5 × 10^{4} naive OT-I CD8^{+} T cells and then infecting them with VSV-OVA. For intravital imaging experiments, we seeded C57BL/6 or CD11c-YFP mice with 5 × 10^{4} GFP^{+}CD8^{+} or CFP^{+}CD8^{+} P14 T cells and then infected the mice with LCMV, with the following exception: to aid analysis, mice for use in experiments on days 4.5 and 8 received a mixture of 4.5 × 10^{4} P14 CD8^{+} T cells and 0.5 × 10^{4} GFP^{+}CD8^{+} P14 T cells. To investigate bystander memory CD8^{+} T cell recruitment and acquisition of the T_{RM} cell phenotype, we purified CD45.1^{+}CD8^{+} OT-I memory T cells from OT-I memory donors (generated by infection with VSV-OVA at least 60 d prior) with a CD8^{+} T cell isolation kit (StemCell Technologies) and injected 1.5 × 10^{6} OT-I CD8^{+} T cells i.v. into a single CD90.1^{+} P14 immune host.

Intravascular staining, lymphocyte isolation and phenotyping

We used an intravascular staining method to discriminate cells present in the vasculature from cells in the tissue parenchyma, as described[43]. We injected mice i.v. with biotin/fluorochrome-conjugated anti-CD8α through the tail vein. Three minutes after the injection, we killed the animals and harvested tissues as described[44]. Isolated mouse cells were surface-stained with antibodies to CD3 (145-2C11), CD45 (30F-11), CD11b (M1/70), CD11c (N418), CD90.1 (OX-7), CD45.1 (A20), MHC II (Ia-Ie) (M5/114.15.2), CD8α (53-6.7), CD8β (YTS156.7.7), CD45.2 (104), CD4 (RM4-5), CD62L (MEL-14), CD44 (IM7), CD69 (H1.2F3) and CD103 (M290), all from BD Biosciences, Biolegend or Affymetrix eBiosciences. Cell viability was determined with Ghost Dye 780 (Tonbo Biosciences). The stained samples were acquired with LSRII or LSR Fortessa flow cytometers (BD) and analyzed with FlowJo software (Treestar).

In vivo BrdU assay

For studies investigating BrdU incorporation, animals were injected i.p. with 2 mg of BrdU (Sigma-Aldrich) 2 h before they were killed for cell isolation. Intracellular staining of cells for BrdU and Ki67 was done with the BD BrdU flow kit (BD Biosciences) with antibodies to BrdU (Bu20a) and Ki67 (SolA15) according to the manufacturer's guidelines.

Tissue freezing, immunofluorescence and microscopy

Harvested mouse tissues were fixed in 2% paraformaldehyde for 2 h before being treated with 30% sucrose overnight for cryoprotection. The sucrose-treated tissue was embedded in OCT tissue-freezing medium and frozen in an isopentane liquid bath. Frozen blocks were processed, stained, imaged, and enumerated by QIM as described[12], including staining with antibodies to the following markers: CD8-β (YTS156.7.7; BD Biosciences), CD90.1 (OX-7; BD Biosciences), CD45.1 (A20; Biolegend), E-cadherin (DECMA-1; Abcam), collagen-IV (goat anti-mouse polyclonal; Millipore), collagen-I (rabbit anti-mouse polyclonal; Millipore), Ki67 (TEC3; Dako), and LCMV nucleoprotein (VL-4; Bioxcell). We also counterstained with 4′,6-diamidino-2-phenylindole dihydrochloride (DAPI) to detect nuclei. The following secondary antibodies were from Jackson Immunoresearch: donkey anti-rabbit (polyclonal), bovine anti-goat (polyclonal), and donkey anti-rat (polyclonal).

Preparation of epidermal whole mounts

We prepared epidermal whole mounts for immunofluorescence as described[45]. We prepared epidermal sheets from back skin by affixing the epidermis side to slides with an optically clear doublesided adhesive (Thorlabs). Slides were incubated in 2.5 mg/ml Dispase II (Roche Diagnostics) in PBS for 1 h at 37°C, and then the dermis was physically removed. Epidermal mounts were fixed in chilled acetone for 5 min. They were subsequently stained, and images were captured as described above. Antigen-specific $CD8^+$ T cells in epidermis were counted manually in Photoshop. The area of the epidermis was measured with the ruler tool in Photoshop.

In vivo antibody treatment and local T_{RM} cell reactivation

We depleted circulating CD90.1^{+}CD8^{+} P14 T cells by injecting 0.6–1.5 μg of titrated anti-CD90.1 (HIS51) i.p. as described[16]. To block the migration of peripheral memory CD8^{+} T cells to the site of reactivation, we injected 500 μg of blocking anti-VCAM-1 (M/K-2.7) or anti-CD49d (PS/2) (BioXcell) i.p. 24 h before and 24 h after trans-cervical peptide challenge as described[16]. For local FRT T_{RM} cell rechallenge experiments involving peptides, 50 μg of the indicated peptides (New England Peptides) was delivered trans-cervically as described[21] in a volume of 30 μl delivered by modified gel loading pipet. For reactivation of skin T_{RM} cells, 3×10^6 PFU of modified vaccinia virus Ankara expressing the SIINFEKL peptide of ovalbumin (MVA-OVA) was delivered epicutaneously into the back skin by 10–15 pokes with a bifurcated needle as described[27]. Reactivation of OT-I T_{RM} cells in FRT was achieved by trans-cervical delivery of either 4×10^6 PFU of VV-OVA or 3×10^6 PFU of MVA-OVA as indicated.

Parabiotic surgery

Parabiotic surgery was done as described[21] with the following modification. Lateral skin incisions on both pairs were conjoined with surgical wound clips. Parabionts were then allowed to rest for 14–30 d before experiments. Equilibration was confirmed in the peripheral blood before T_{RM} cell reactivation.

Two-photon microscopy and analysis

Mice were anesthetized with 2,2,2-tribromoethanol (Avertin), and uterine horns were located through a midline incision along the linea alba. One uterine horn was gently exteriorized and positioned on a custom-made polystyrene platform, where it was stabilized with cyanoacrylate tissue adhesive. The platform allowed constant bathing of the organ in warm oxygenated buffer and permitted continuous temperature monitoring. The mouse was then transferred onto a microscope stage fully enclosed within an environmental chamber that helped maintain body temperature at 36.5 ± 1°C. Mice were injected with 50 μl of rhodamine isothiocyanate, 70 K_d (20 mg/ml stock), where indicated to visualize blood vessels.

Movies were acquired with an MP SP5 two-photon microscope TCS (Leica) equipped with Mai Tai HP DeepSee lasers (SpectraPhysics), an 8,000-Hz resonant scanner, a 25 × /0.95-NA (numerical aperture) objective, and two NDD and two HyD photomultiplier tubes. Samples were excited at 860 or 890 nm, and multiple fluorophores were imaged with the custom dichroic mirrors with the following collections: SHG, < 440 nm; CFP, 435–485 nm; GFP, 500–520 nm; YFP, 520–550 nm; and rhodamine dextran, 565–605 nm. All imaging studies focused on the perimetrium and myometrium regions of the uterus. Imaging data were processed with Imaris software (versions 7.6.4 and 8.0.1). For the calculation in Fig. 1g, a surface was created for SHG signal and then converted to a distance transformation channel to determine spot distance to the SHG surface at all time points. Determination of mean track velocities (in micrometers per minute) and motility coefficients and other migrational analyses were carried out with MotilityLab (http://www.motilitylab.net/) or a macro[46]. The drift correct function in Imaris and MotilityLab was used to correct for uterine tissue contractions during imaging. In cases where uterine tissue contractions were severe,

we injected terbutaline hemisulfate (Sigma-Aldrich), a β-adrenergic agonist, i.p. at 50 mg/kg body weight to achieve transient uterine muscle relaxation. No adverse effect on $CD8^+$ T cell surveillance behavior was noted during this short-term terbutaline treatment.

Bone marrow chimeras and diphtheria toxin treatment

Bone marrow was harvested from femurs and tibias of CD11c-DTR mice, and $1–2 \times 10^6$ bone marrow cells were injected i.v. into recipient mice that had received a lethal irradiation dose of 1,100 cGy. Mice received antibiotics in drinking water for 4 weeks after irradiation and were allowed 8 weeks for full reconstitution of bone marrow, which was confirmed by analysis of donor peripheral cells. We depleted $CD11c^+$ cells in the chimeric mice by treating them with an initial dose of 1 μg of DT i.p. and then 0.2 μg of DT i.p. every 2 d until the end of the experiment.

Statistics

If the samples followed a Gaussian distribution, then parametric tests (unpaired two-tailed Student's *t*-test for two groups and one-way ANOVA with Tukey's multiple comparison test for more than two groups) were used. If the samples deviated from a Gaussian distribution, non-parametric tests (Mann-Whitney *U*-test for two groups, Kruskal-Wallis with Dunn's multiple comparison test for more than two groups) were used unless otherwise stated. The DAgostino and Pearson omnibus normality test was used to determine whether samples adhered to a Gaussian distribution. Variances between groups were compared by *F* test and found to be equal. All statistical analysis was done in GraphPad Prism (GraphPad Software Inc.). $P < 0.05$ was considered significant.

Life Sciences Reporting Summary

Further information on experimental design is available in the Life Sciences Reporting Summary.

Data availability

The data that support the findings of this study are available from the corresponding author upon request.

Supplementary Material

Refer to Web version on PubMed Central for supplementary material.

Acknowledgments

We thank the members of the Masopust laboratory for helpful discussions. This work was funded by the Howard Hughes Medical Institute Faculty Scholars program (D.M.) and the US National Institutes of Health (grants R01AI111671 and R01AI084913 to D.M.; grant R21AI123600 to B.J.B.). H.D.H. was funded by the Intramural Research Program of the US National Institute of Allergy and Infectious Diseases.

References

1. von Andrian UH, Mackay CR. T-cell function and migration. Two sides of the same coin. N Engl J Med. 2000; 343:1020–1034. [PubMed: 11018170]

2. Mueller SN, Gebhardt T, Carbone FR, Heath WR. Memory T cell subsets, migration patterns, and tissue residence. Annu Rev Immunol. 2013; 31:137–161. [PubMed: 23215646]
3. Stemberger C, et al. Stem cell-like plasticity of naive and distinct memory $CD8^+$ T cell subsets. Semin Immunol. 2009; 21:62–68. [PubMed: 19269852]
4. Wherry EJ, et al. Lineage relationship and protective immunity of memory CD8 T cell subsets. Nat Immunol. 2003; 4:225–234. [PubMed: 12563257]
5. Farber DL, Yudanin NA, Restifo NP. Human memory T cells: generation, compartmentalization and homeostasis. Nat Rev Immunol. 2014; 14:24–35. [PubMed: 24336101]
6. Sallusto F, Geginat J, Lanzavecchia A. Central memory and effector memory T cell subsets: function, generation, and maintenance. Annu Rev Immunol. 2004; 22:745–763. [PubMed: 15032595]
7. Park CO, Kupper TS. The emerging role of resident memory T cells in protective immunity and inflammatory disease. Nat Med. 2015; 21:688–697. [PubMed: 26121195]
8. Mueller SN, Mackay LK. Tissue-resident memory T cells: local specialists in immune defence. Nat Rev Immunol. 2016; 16:79–89. [PubMed: 26688350]
9. Mowat AM, McInnes IB, Parrott DMV. Functional properties of intra-epithelial lymphocytes from mouse small intestine. IV Investigation of the proliferative capacity of IEL using phorbol ester and calcium ionophore. Immunology. 1989; 66:398–403. [PubMed: 2495248]
10. Ebert EC, Roberts AI, Brolin RE, Raska K. Examination of the low proliferative capacity of human jejunal intraepithelial lymphocytes. Clin Exp Immunol. 1986; 65:148–157. [PubMed: 2947761]
11. Masopust D, Vezys V, Wherry EJ, Barber DL, Ahmed R. Cutting edge: gut microenvironment promotes differentiation of a unique memory CD8 T cell population. J Immunol. 2006; 176:2079–2083. [PubMed: 16455963]
12. Steinert EM, et al. Quantifying memory CD8 T cells reveals regionalization of immunosurveillance. Cell. 2015; 161:737–749. [PubMed: 25957682]
13. Fernandez-Ruiz D, et al. Liver-resident memory $CD8^+$ T cells form a frontline defense against malaria liver-stage infection. Immunity. 2016; 45:889–902. [PubMed: 27692609]
14. Wakim LM, et al. The molecular signature of tissue resident memory CD8 T cells isolated from the brain. J Immunol. 2012; 189:3462–3471. [PubMed: 22922816]
15. Ariotti S, et al. Skin-resident memory $CD8^+$ T cells trigger a state of tissue-wide pathogen alert. Science. 2014; 346:101–105. [PubMed: 25278612]
16. Schenkel JM, et al. Resident memory CD8 T cells trigger protective innate and adaptive immune responses. Science. 2014; 346:98–101. [PubMed: 25170049]
17. Gebhardt T, et al. Different patterns of peripheral migration by memory $CD4^+$ and $CD8^+$ T cells. Nature. 2011; 477:216–219. [PubMed: 21841802]
18. Zaid A, et al. Persistence of skin-resident memory T cells within an epidermal niche. Proc Natl Acad Sci USA. 2014; 111:5307–5312. [PubMed: 24706879]
19. Miller MJ, Wei SH, Parker I, Cahalan MD. Two-photon imaging of lymphocyte motility and antigen response in intact lymph node. Science. 2002; 296:1869–1873. [PubMed: 12016203]
20. Casey KA, et al. Antigen-independent differentiation and maintenance of effector-like resident memory T cells in tissues. J Immunol. 2012; 188:4866–4875. [PubMed: 22504644]
21. Schenkel JM, Fraser KA, Vezys V, Masopust D. Sensing and alarm function of resident memory $CD8^+$ T cells. Nat Immunol. 2013; 14:509–513. [PubMed: 23542740]
22. Beura LK, et al. Lymphocytic choriomeningitis virus persistence promotes effector-like memory differentiation and enhances mucosal T cell distribution. J Leukoc Biol. 2015; 97:217–225. [PubMed: 25395301]
23. Nakanishi Y, Lu B, Gerard C, Iwasaki A. $CD8^+$ T lymphocyte mobilization to virus-infected tissue requires $CD4^+$ T-cell help. Nature. 2009; 462:510–513. [PubMed: 19898495]
24. Jiang X, et al. Skin infection generates non-migratory memory $CD8^+$ T_{RM} cells providing global skin immunity. Nature. 2012; 483:227–231. [PubMed: 22388819]
25. Sun JC, Bevan MJ. Defective CD8 T cell memory following acute infection without CD4 T cell help. Science. 2003; 300:339–342. [PubMed: 12690202]

26. Shedlock DJ, Shen H. Requirement for CD4 T cell help in generating functional CD8 T cell memory. Science. 2003; 300:337–339. [PubMed: 12690201]
27. Hickman HD, et al. Anatomically restricted synergistic antiviral activities of innate and adaptive immune cells in the skin. Cell Host Microbe. 2013; 13:155–168. [PubMed: 23414756]
28. Gaylo A, Schrock DC, Fernandes NRJ, Fowell DJ. T cell interstitial migration: motility cues from the inflamed tissue for micro- and macro-positioning. Front Immunol. 2016; 7:428. [PubMed: 27790220]
29. Weninger W, Biro M, Jain R. Leukocyte migration in the interstitial space of non-lymphoid organs. Nat Rev Immunol. 2014; 14:232–246. [PubMed: 24603165]
30. Steinbach K, et al. Brain-resident memory T cells represent an autonomous cytotoxic barrier to viral infection. J Exp Med. 2016; 213:1571–1587. [PubMed: 27377586]
31. Glennie ND, et al. Skin-resident memory $CD4^+$ T cells enhance protection against *Leishmania major* infection. J Exp Med. 2015; 212:1405–1414. [PubMed: 26216123]
32. Stary G, et al. A mucosal vaccine against *Chlamydia trachomatis* generates two waves of protective memory T cells. Science. 2015; 348:aaa8205. [PubMed: 26089520]
33. Khan TN, Mooster JL, Kilgore AM, Osborn JF, Nolz JC. Local antigen in nonlymphoid tissue promotes resident memory $CD8^+$ T cell formation during viral infection. J Exp Med. 2016; 213:951–966. [PubMed: 27217536]
34. Mackay LK, et al. Long-lived epithelial immunity by tissue-resident memory T (T_{RM}) cells in the absence of persisting local antigen presentation. Proc Natl Acad Sci USA. 2012; 109:7037–7042. [PubMed: 22509047]
35. Wu T, et al. Lung-resident memory CD8 T cells (T_{RM}) are indispensable for optimal cross-protection against pulmonary virus infection. J Leukoc Biol. 2014; 95:215–224. [PubMed: 24006506]
36. Çuburu N, et al. Intravaginal immunization with HPV vectors induces tissue-resident $CD8^+$ T cell responses. J Clin Invest. 2012; 122:4606–4620. [PubMed: 23143305]
37. Kang SS, et al. Migration of cytotoxic lymphocytes in cell cycle permits local MHC I-dependent control of division at sites of viral infection. J Exp Med. 2011; 208:747–759. [PubMed: 21464219]
38. Klein I, Crispe IN. Complete differentiation of $CD8^+$ T cells activated locally within the transplanted liver. J Exp Med. 2006; 203:437–447. [PubMed: 16476766]
39. Wakim LM, Waithman J, van Rooijen N, Heath WR, Carbone FR. Dendritic cell-induced memory T cell activation in nonlymphoid tissues. Science. 2008; 319:198–202. [PubMed: 18187654]
40. Posavad CM, et al. Enrichment of herpes simplex virus type 2 (HSV-2) reactive mucosal T cells in the human female genital tract. Mucosal Immunol. 2017; 10:1259–1269. [PubMed: 28051084]
41. Zhu J, et al. Immune surveillance by $CD8\alpha\alpha^+$ skin-resident T cells in human herpes virus infection. Nature. 2013; 497:494–497. [PubMed: 23657257]
42. Clark RA. Resident memory T cells in human health and disease. Sci Transl Med. 2015; 7:269rv1.
43. Anderson KG, et al. Intravascular staining for discrimination of vascular and tissue leukocytes. Nat Protoc. 2014; 9:209–222. [PubMed: 24385150]
44. Thompson EA, Beura LK, Nelson CE, Anderson KG, Vezys V. Shortened intervals during heterologous boosting preserve memory CD8 T cell function but compromise longevity. J Immunol. 2016; 196:3054–3063. [PubMed: 26903479]
45. Mohammed J, et al. Stromal cells control the epithelial residence of DCs and memory T cells by regulated activation of TGF-β. Nat Immunol. 2016; 17:414–421. [PubMed: 26901152]
46. Fife BT, et al. Interactions between PD-1 and PD-L1 promote tolerance by blocking the TCR-induced stop signal. Nat Immunol. 2009; 10:1185–1192. [PubMed: 19783989]

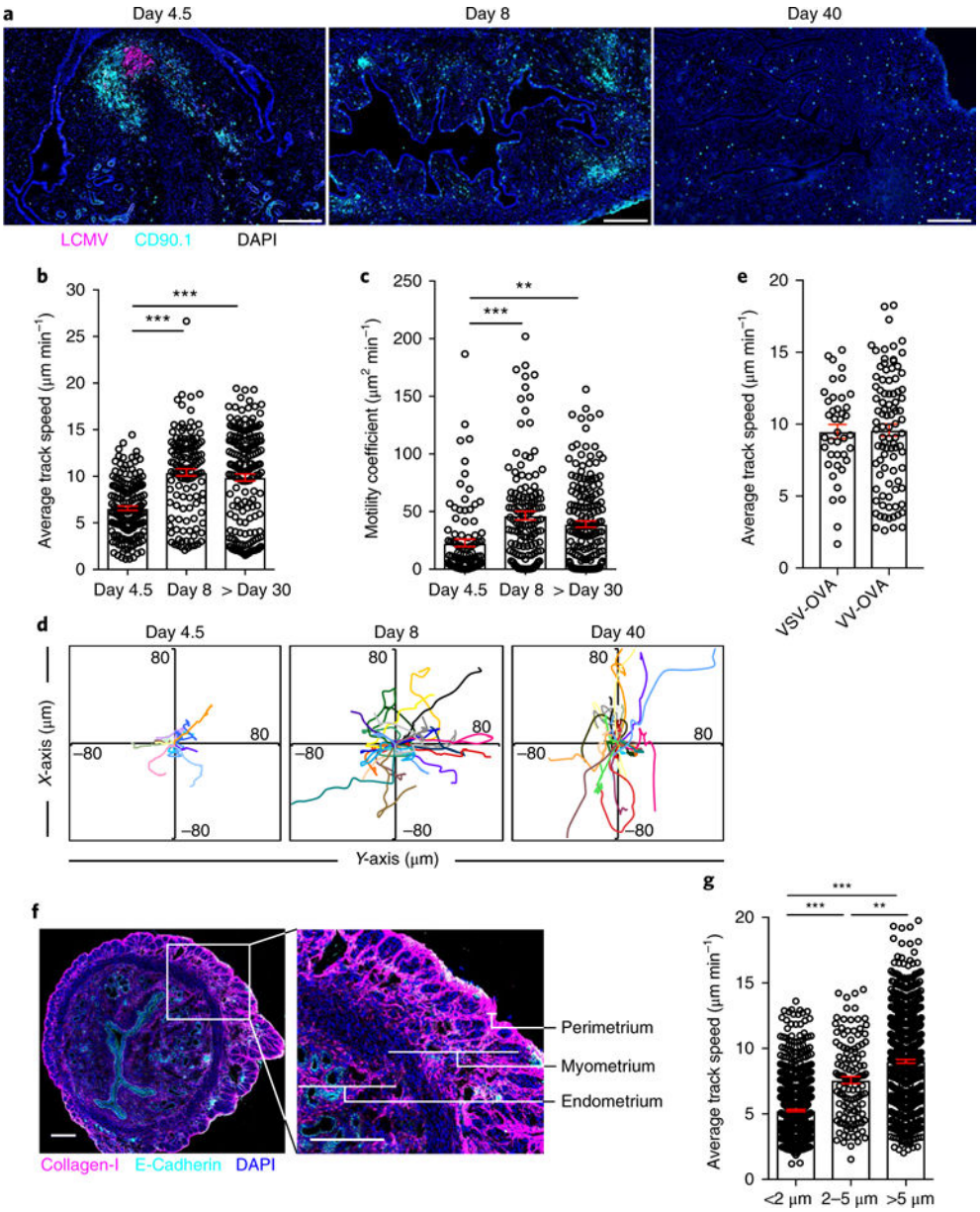

Fig. 1. Migration of CD8$^+$ T cells in the FRT

a, CD90.1$^+$GFP$^+$CD8$^+$ P14 T cells were transferred to female C57BL/6J mice 1 d before Infection with LCMV Armstrong. We stained the FRT with DAPI (blue), anti-CD90.1 (to label P14; cyan) and anti-LCMV nucleoprotein (magenta) 4.5, 8 or 40 d later. Scale bars, 200 μm. **b**,**c**, The average track speed (**b**) and motility coefficients (**c**) of GFP$^+$CD8$^+$ P14 T cells in the FRT on the indicated days after LCMV infection, as determined by intravital microscopy. **d**, Flower plots of 2D tracks of several GFP$^+$CD8$^+$ P14 T cells, superimposed after normalization of their starting coordinates to the origin. **e**, GFP$^+$CD8$^+$ OT-I T cells were transferred to female C57BL/6J mice 1 d before infection with VSV-OVA or VV-OVA. The plot shows the average track speed of GFP$^+$CD8$^+$ OT-I T cells in the uterine horn 60 d after the respective infections. **f**, Transverse sections of mouse uterine horn stained for collagen-l (magenta), E-cadherin (cyan) and nuclei (DAPI; blue). Part of the section on the

left (white rectangle) is shown at higher magnification on the right, depicting three layers of uterine horn with different collagen densities. Scale bars, 200 μm. **g**, $CD8^+$ P14 memory T cell track speeds binned into three groups (<2 μm, 2–5 μm and >5 μm) on the basis of their average distance from the collagen (SHG) surface. Data in **b**,**c**,**e**,**g** are shown as mean ± s.e.m.; circles represent individual cells. $^{**}P<0.01$, $^{***}P< 0.001$, Kruskal-Wallis one-way analysis of variance (ANOVA) with Dunn's multiple comparison test. Data are representative of two independent experiments with $n = 4$ mice per infection (**a**,**f**) or three separate experiments with $n = 3$ mice per group per experiment (**b**,**c**,**e**,**g**).

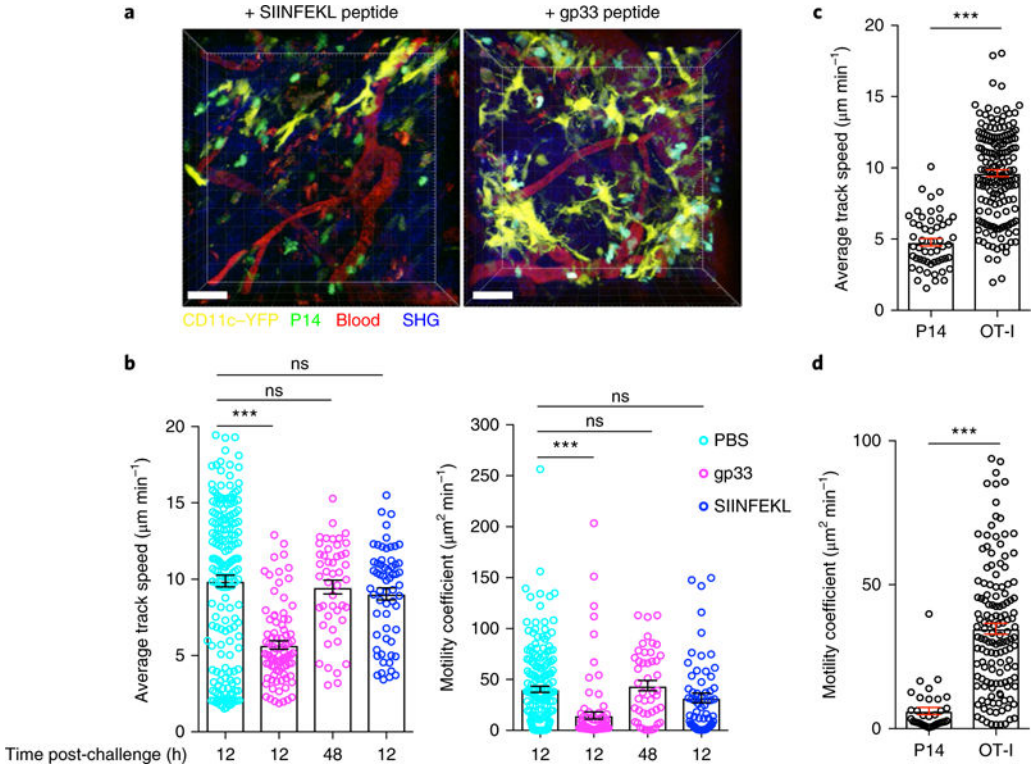

Fig. 2. Motility arrest by T_{RM} cells after cognate antigen interaction

a, To assess in situ T_{RM} cell reactivation, we transferred naive GFP^+CD8^+ P14 T cells into female C57BL/6J mice 1 d before infection with LCMV Armstrong, and 60 d later we challenged the mice trans-cervically with PBS, P14 reactivating peptide gp33 or control peptide SIINFEKL. Shown are representative snapshots, from Supplementary Videos 4 and 5, of the maximal projection of 3D z-stack images of P14 immune chimeras 12 h after trans-cervical exposure to peptide. Green, GFP^+CD8^+ P14 T cells; yellow, $CD11c^+$ dendritic cells. Scale bars, 40 μm. **b**, Average track speed and motility coefficients of GFP^+CD8^+ P14 T cells 12 h or 48 h after trans-cervical challenge with the indicated peptide. **c**,**d**, To assess the motility of a bystander population of memory T cells, we transferred CFP^+CD8^+ P14 T cells into naive mice 1 d before LCMV infection. Thirty days later, we transferred GFP^+CD8^+ OT-I T cells into these LCMV immune chimeras, and then infected them with VSV-OVA. Thirty days after VSV-OVA infection (60 d after LCMV infection), we challenged these double-immune chimeras trans-cervically with gp33 peptide, and carried out intravital microscopy 12 h after challenge. The average track speed (**c**) and motility coefficients (**d**) of P14 and OT-I $CD8^+$ T cells 12 h after gp33 peptide challenge are shown. Data are representative of two separate experiments with 4 mice per group per experiment. ***$P<$ 0.001; ns, not significant; Kruskal-Wallis ANOVA with Dunn's multiple comparison test (**b**) or Mann-Whitney *U*-test (**c**,**d**). Data in **b**-**d** are shown as the mean ± s.e.m.; circles represent individual cells.

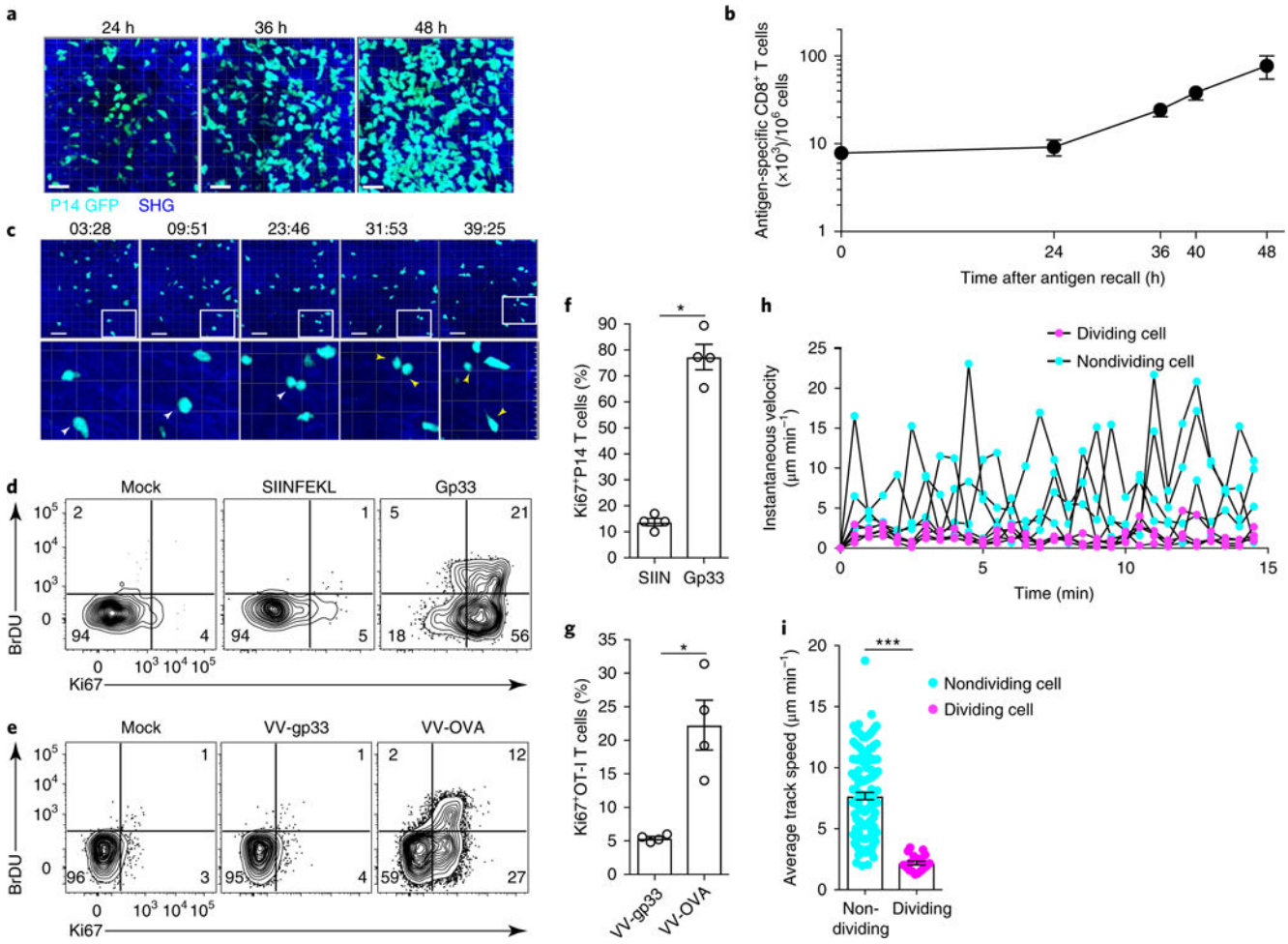

Fig. 3. In situ division of CD8$^+$ T cells in the FRT

a,**b**, Accumulation of P14 CD8$^+$ T cells after local T_{RM} cell reactivation in FRT. **a**, Representative maximal projections of 3D z-stack images of GFP$^+$CD8$^+$ P14 T cells (cyan) after trans-cervical challenge with gp33. Scale bars, 30 μm. **b**, The abundance of P14 CD8$^+$ T cells enumerated by QIM in 7-μm sections of FRT. **c**, Top, representative time-lapse images (time stamps in minutes and seconds are shown above the images) of GFP$^+$CD8$^+$ P14 T cells (cyan) undergoing division beginning ~36 h after gp33 challenge. Scale bars, 40 μm. Bottom, magnified views (4× magnification compared with the images above) of dividing cells, indicated by white arrowheads (or two yellow arrowheads for cells after cytokinesis). Magnified cells are outlined by white rectangles in the images above. **d**, P14 immune chimeras were challenged with peptides (gp33 or SIINFEKL) or mock-challenged (with PBS), and tissues were harvested 48 h after challenge. Animals received 2 mg of BrdU i.p. before cell collection. **e**, OT-I immune chimeras were challenged with viruses (VV-OVA and VV-gp33) or mock-challenged, and tissues were harvested 48 h after recall. In **d** and **e**, numbers in corners indicate the percentage of cells in each quadrant. **f**,**g**, The frequency of Ki67$^+$ cells in FRT of the mice described in **d** (see **f**) and **e** (see **g**). SIIN, SIINFEKL. **h**, Instantaneous track speed versus time, beginning 15min before cytokinesis, for four representative dividing and four nondividing P14 CD8$^+$ T cells. **i**, The mean track speed of

dividing and nondividing cells 36h after recall. *P< 0.05, ***P< 0.001, Mann-Whitney U-test. Data in **b**,**f-i** are shown as the mean ± s.e.m. Data are representative of two separate experiments with 3 (**a**,**b**) or 4 (**f**,**g**) mice per group per experiment or are pooled from 6 individual movies and 3 animals (**i**).

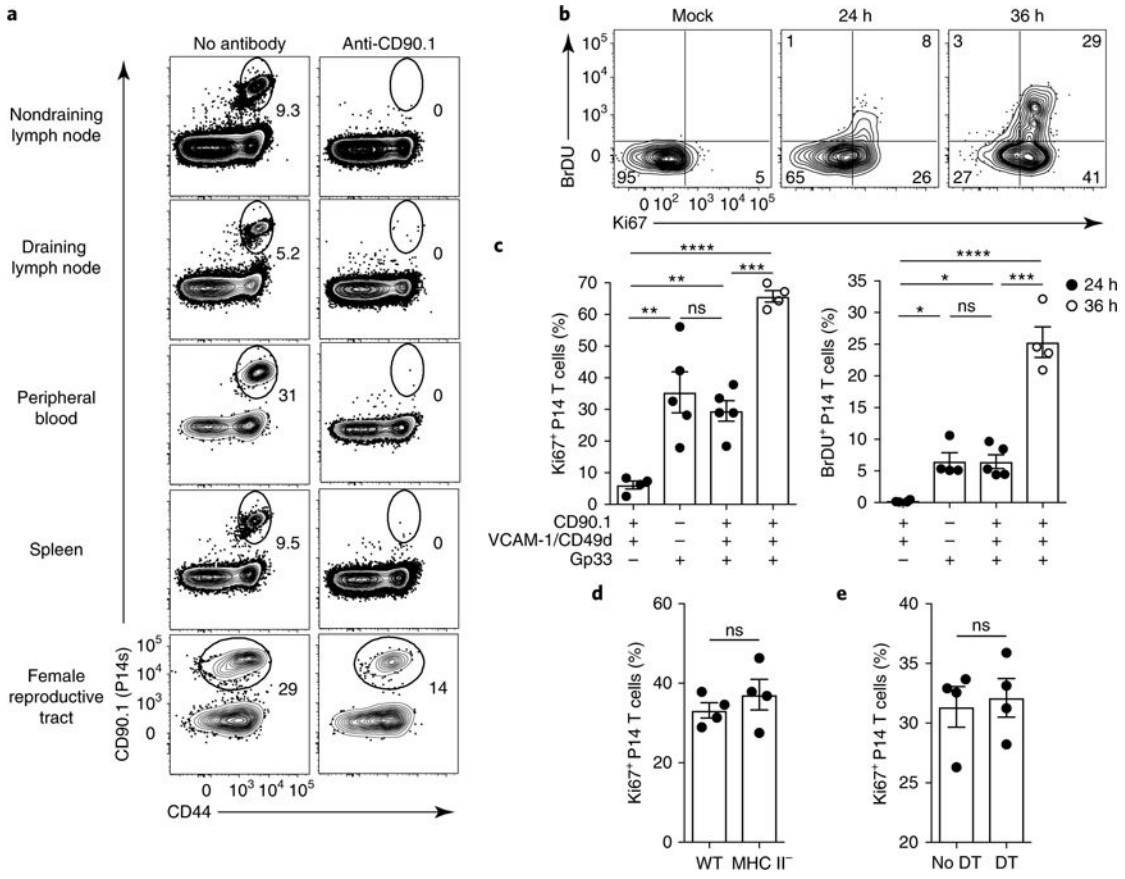

Fig. 4. T_{RM} cells initiate division in mucosae after reactivation

a, The presence of remaining P14 memory $CD8^+$ T cells in the indicated tissues 4 d after i.p. anti-CD90.1 treatment in P14 LCMV immune chimeric mice. Numbers indicate the percentage of cells in the gate. **b**, P14 immune chimeras were treated as in **a**. Their blood was assessed for successful depletion of P14 $CD8^+$ T cells 4 d later, and they received anti-VCAM-1 and anti-CD49d i.p. on day 4. On day 5, mice were rechallenged trans-cervically with gp33 peptide or PBS (Mock), and they were assessed 24h or 36 h after rechallenge. Mice received 2 mg of BrdU i.p. 2 h before they were killed, and P14 $CD8^+$ T cells isolated from FRT were stained for Ki67 and BrdU incorporation by flow cyotmetry. Numbers in corners indicate the percentage of cells in the gate. **c**, The percentage of $Ki67^+$ or $BrdU^+$ cells among P14 $CD8^+$ T cells isolated from the FRT of mice treated with anti-CD90.1, anti-VCAM-1, anti-CD49d and gp33 as indicated. Data points represent individual mice. **d**, $Ki67^+CD8^+$ P14 T cell frequency as enumerated by flow cytometry 24h after challenge in wild-type (WT) and MHC-II-deficient P14 immune chimeric mice treated as in **b**. **e**, P14 immune chimeras were generated in CD11c-DTR chimeric mice. Sixty days later, mice were either treated with diphtheria toxin (every 48 h starting 2 d before recall) or left untreated. The mice were also treated with antibodies to CD90.1, VCAM-1, CD49d and gp33 peptide as in **b** and **c**. The plot shows the percentage of $Ki67^+CD8^+$ P14 T cells isolated from FRT as determined by flow cytometry 24 h after challenge. ns, not significant; $*P<0.05$, $**P<0.01$, $***P<0.001$, $****P<0.0001$; Kruskal-Wallis ANOVA (**c**) or Mann-Whitney *U*-test (**d**,**e**). Data in **c**–**e** are shown as the mean ± s.e.m. Data are representative of two separate

experiments with 3 (**a**) or 4 (**d**,**e**) mice per group per experiment, or three separate experiments with 4 mice per group per experiment (**b**,**c**).

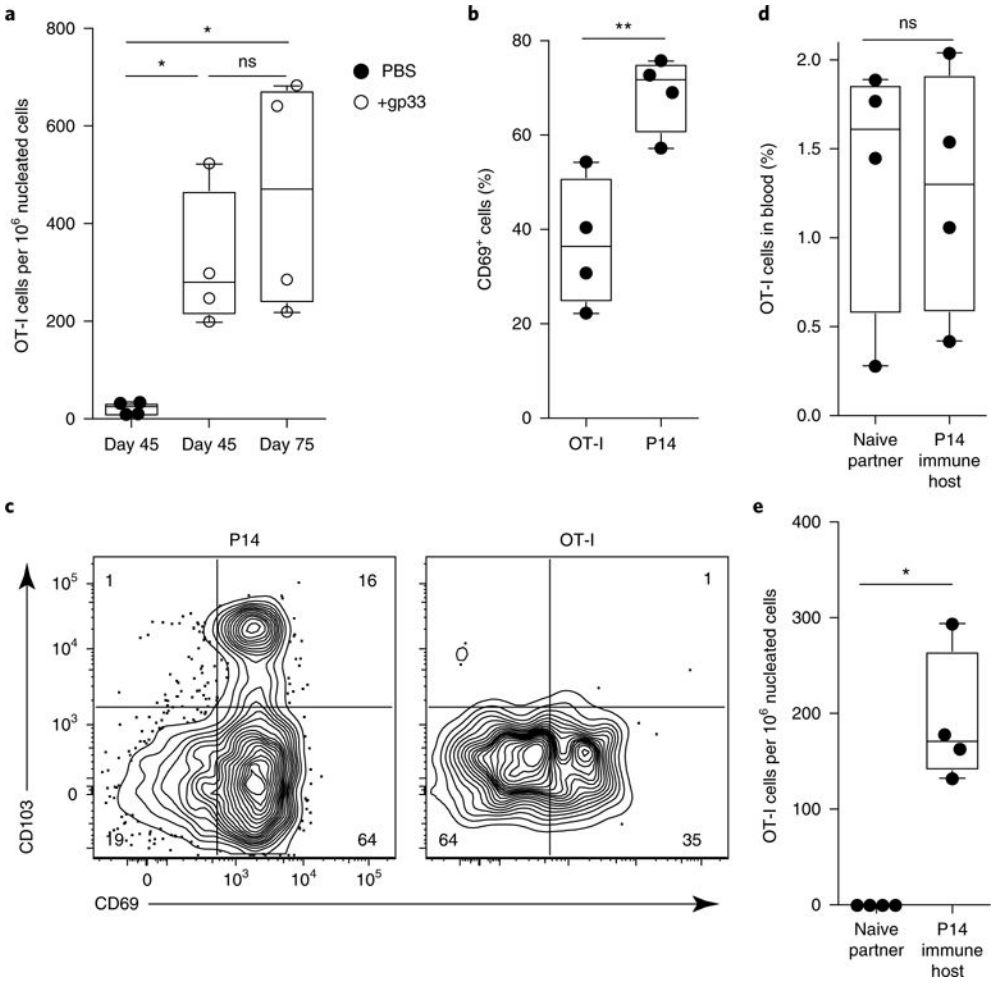

Fig. 5. Recruited circulating bystander memory CD8$^+$ T cells adopt a T_{RM} cell phenotype

a, To pull non-antigen-specific recirculating OT-I memory cells to the FRT, we transferred OT-I memory CD8$^+$ T cells i.v. into P14 immune chimeras. The next day, we challenged recipients trans-cervically with PBS (mock) or gp33 peptide. Mice were rested until day 45 or day 75, at which time we used QIM to enumerate OT-I CD8$^+$ T cells in the FRT. **b**, The frequency of FRT OT-I or P14 CD8$^+$ T cells that were CD69$^+$, as evaluated by flow cytometry. **c**, Representative flow cytometry plots of CD69 and CD103 staining on P14 and OT-I CD8$^+$ T cells 45 d after recall. Numbers in corners indicate the percentage of cells in each quadrant. **d**,**e**, To confirm that recruited OT-I CD8$^+$ T cells were resident, we carried out parabiotic surgery to conjoin mice treated 40 d prior with trans-cervical gp33 peptide as described above (P14 immune hosts) with naive B6 partner mice. We examined each parabiont for the presence of OT-I CD8$^+$ T cells in blood and FRT 35 d after surgery. *P<0.05, **P< 0.01, Kruskal-Wallis ANOVA (**a**) or Mann-Whitney U-test (**b**,**d**,**e**). Box plots indicate medians (center lines), 25th and 75th percentiles (bottom and top box edges, respectively), minima and maxima (whiskers), and individual data points (circles). Data are representative of three separate experiments with 4 mice per group per experiment (**a**–**c**) or two separate experiments with four parabiont pairs per experiment (**d**,**e**).

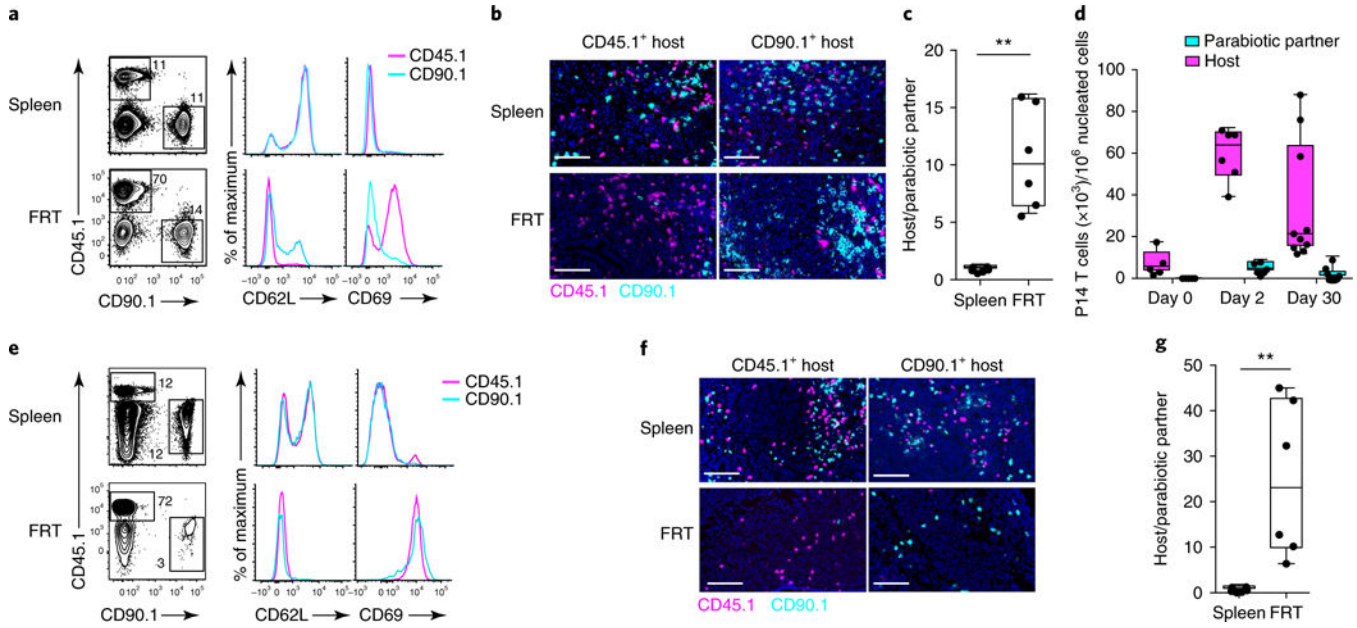

Fig. 6. T_{RM} cell proliferation dominates expansion of local secondary memory T cell populations

a, Equilibration of recirculating memory $CD8^+$ T cells in parabiotically conjoined $CD45.1^+$ and $CD90.1^+$ P14 immune chimeras challenged trans-cervically with gp33 peptide 14–30 d after surgery. Scale bars, 50 μm. **a**–**g**, We analyzed spleen and FRT by flow cytometry 2 d (**a**) or 30 d (**e**) after gp33 challenge to evaluate the relative contributions of host and donor P14 $CD8^+$ T cells to the secondary response. Tissues from a $CD45.1^+$ immune chimera are shown, and histograms indicate phenotypes of gated $CD45.1^+$ and $CD90.1^+$ P14 $CD8^+$ T cells at day 2 (**a**) or day 30 (**e**) post-recall. $CD45.1^+$ and $CD90.1^+$ P14 $CD8^+$ T cells were also analyzed in each parabiont by immunofluorescence staining 2 d (**b**) and 30 d (**f**) after t.c. gp33 challenge. **d**, Host and parabiotic partner P14 $CD8^+$ T cells enumerated by QIM on the indicated days after trans-cervical gp33 challenge. **c**,**g**, The ratio of host and parabiotic partner P14 $CD8^+$ T cells in each parabiont 2 d (**c**) and 30 d (**g**) after trans-cervical peptide recall. All data are representative of two separate experiments with at least four parabiont pairs/time points, with a total of > 16 individual mice in individual groups. $^{**}P<0.01$, Mann-Whitney *U*-test. In **a** and **e**, numbers adjacent to outlines indicate the percentage of cells in the gate. Box plots indicate medians (center lines), 25th and 75th percentiles (bottom and top box edges, respectively), minima and maxima (whiskers), and individual data points (circles).

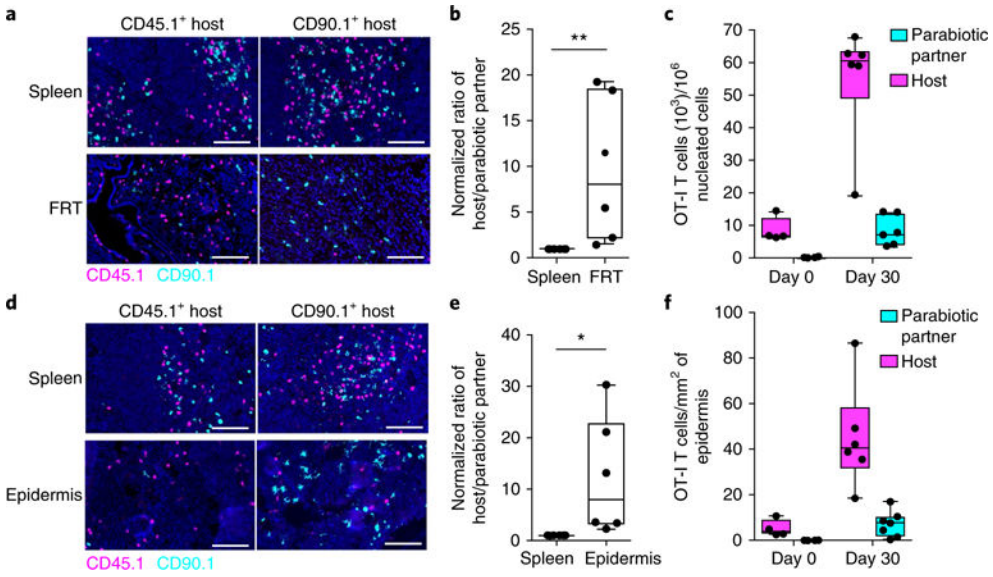

Fig. 7. T_{RM} cell proliferation dominates expansion of local secondary memory T cell populations after FRT or skin rechallenge

a, Tissues from VSV-OVA-immunized CD45.1$^+$ and CD90.1$^+$ OT-I immune chimeras that were surgically conjoined by parabiosis to achieve equilibration of recirculating memory CD8$^+$ T cells. **a**–**f**, Both parabionts were challenged with MVA-OVA 14–30 d after surgery via either the (**a**–**c**) trans-cervical or (**d**–**f**) epicutaneous route. OT-I CD8$^+$ T cells were analyzed by immunofluorescence staining and enumerated by QIM in either FRT (**b**,**c**) or skin epidermis (**e**,**f**) and in the spleen 30 d after rechallenge. Magenta, CD45.1; cyan, CD90.1; blue, DAPI (nuclei). Scale bars, 50 μm. Ratios of host and donor-derived OT-I CD8$^+$ T cells were calculated after normalization to the respective ratios in spleen. Absolute numbers of OT-I CD8$^+$ T cells in FRT (**c**) and skin epidermis (**f**) in unchallenged and MVA-OVA-challenged (30 d post-recall) mice are shown. All data are representative of two separate experiments with three parabiont pairs per experiment, with a total of 12 individual mice in individual groups. *P< 0.05, **P<0.01, Mann-Whitney U-test (**b**) or unpaired t-test (**e**). Box plots indicate medians (center lines), 25th and 75th percentiles (bottom and top box edges, respectively), minima and maxima (whiskers), and individual data points (circles).